https://doi.org/10.15302/frontphys.2025.044204

Supplementary Information: Realization of a non-Hermitian Haldane model in circuits

Rujiang Li[1],* Wencai Wang[1], Xiangyu Kong[1], Bo Lv[2], Yongtao Jia[1], Huibin Tao[3],† Pengfei Li[4,5], and Ying Liu[1]
[1]*National Key Laboratory of Radar Detection and Sensing, School of Electronic Engineering, Xidian University, Xi'an 710071, China*
[2]*Key Laboratory of In-Fiber Integrated Optics of Ministry of Education, College of Physics and Optoelectronic Engineering, Harbin Engineering University, Harbin 150001, Heilongjiang Province, China*
[3]*School of Software Engineering, Xi'an Jiaotong University, Xi'an, China*
[4]*Department of Physics, Taiyuan Normal University, Jinzhong, 030619, China and*
[5]*Institute of Computational and Applied Physics, Taiyuan Normal University, Jinzhong, 030619, Shanxi, China*

Supplementary Note 1. Circuit Hamiltonian. The Hamiltonian for the Haldane model on a honeycomb lattice is $\mathbf{H}=\omega_{\mathrm{A,B}}\sum_i c_i^{\dagger}c_i+t_1\sum_{\langle i,j\rangle}\left(c_i^{\dagger}c_j+c_j^{\dagger}c_i\right)+t_2\sum_{\langle\langle i,j\rangle\rangle}\left(e^{i\phi}c_i^{\dagger}c_j+e^{-i\phi}c_j^{\dagger}c_i\right)$, where $\omega_{\mathrm{A,B}}$ are the on-site staggering energies, t_1 is the NN hopping, and $t_2e^{\pm i\phi}$ is the NNN hopping. The circuit lattice shown in Fig. 1b emulates the Haldane model. We deform the circuit lattice in Fig. 1b to a brick wall structure, as shown in Fig. S1 [1]. In the general case of $\delta\nu\neq 0$, according to Kirchhoff's law, the voltages $\mathbf{V}$ at the circuit nodes are related to the input currents $\mathbf{I}$ by

$$\begin{aligned}
I_{\mathrm{A}}(x,y)=&\frac{1}{-i\omega L_{\mathrm{g}}}V_{\mathrm{A}}(x,y)-i\omega\left(C_{\mathrm{A}}+3C\right)V_{\mathrm{A}}(x,y)\\
&+i\omega C\left[V_{\mathrm{B}}\left(x-\frac{1}{2},y\right)+V_{\mathrm{B}}\left(x+\frac{1}{2},y\right)+V_{\mathrm{B}}\left(x+\frac{1}{2},y-1\right)\right]\\
&+\left(\frac{1}{R_{\mathrm{g}}}+\frac{3\nu_1}{R}-\frac{3\nu_2}{R}\right)V_{\mathrm{A}}(x,y)\\
&-\frac{\nu_1}{R}\left[V_{\mathrm{A}}(x-1,y)+V_{\mathrm{A}}(x,y+1)+V_{\mathrm{A}}(x+1,y-1)\right]\\
&+\frac{\nu_2}{R}\left[V_{\mathrm{A}}(x+1,y)+V_{\mathrm{A}}(x,y-1)+V_{\mathrm{A}}(x-1,y+1)\right],
\end{aligned}\tag{S1}$$

$$\begin{aligned}
I_{\mathrm{B}}(x,y)=&\frac{1}{-i\omega L_{\mathrm{g}}}V_{\mathrm{B}}(x,y)-i\omega\left(C_{\mathrm{B}}+3C\right)V_{\mathrm{B}}(x,y)\\
&+i\omega C\left[V_{\mathrm{A}}\left(x-\frac{1}{2},y\right)+V_{\mathrm{A}}\left(x+\frac{1}{2},y\right)+V_{\mathrm{A}}\left(x-\frac{1}{2},y+1\right)\right]\\
&+\left(\frac{1}{R_{\mathrm{g}}}+\frac{3\nu_2}{R}-\frac{3\nu_1}{R}\right)V_{\mathrm{B}}(x,y)\\
&+\frac{\nu_1}{R}\left[V_{\mathrm{B}}(x-1,y)+V_{\mathrm{B}}(x,y+1)+V_{\mathrm{B}}(x+1,y-1)\right]\\
&-\frac{\nu_2}{R}\left[V_{\mathrm{B}}(x+1,y)+V_{\mathrm{B}}(x,y-1)+V_{\mathrm{B}}(x-1,y+1)\right].
\end{aligned}\tag{S2}$$

If periodic boundary conditions are imposed in both the x- and y-directions, the circuit Laplacian $\mathbf{J}$, defined by the relationship $\mathbf{I}=\mathbf{JV}$, can be expressed in reciprocal space as

$$\mathbf{J}=i\sum_{j=0}^{3}d_j\sigma_j,\tag{S3}$$

where

$$d_0=\frac{1}{\omega L_{\mathrm{g}}}-\omega C_{\mathrm{g}}-i\frac{1}{R_{\mathrm{g}}}-3\omega C,\tag{S4}$$

$$d_1=\omega C\left[1+\cos k_x+\cos\left(k_x-k_y\right)\right],\tag{S5}$$

$$d_2=\omega C\left[\sin k_x+\sin\left(k_x-k_y\right)\right],\tag{S6}$$

$$d_3=-\omega\delta C-i\frac{6\delta\nu}{R}+i\frac{2\delta\nu}{R}\left[\cos k_x+\cos k_y+\cos\left(k_x-k_y\right)\right]+\frac{2\nu}{R}\left[\sin k_x-\sin k_y-\sin\left(k_x-k_y\right)\right].\tag{S7}$$

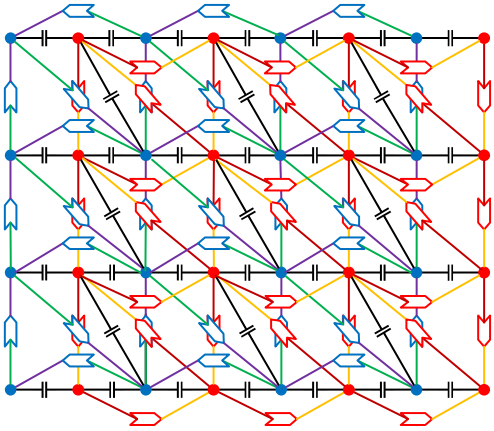

Supplementary Figure S1. Schematic representation of the deformed circuit lattice.

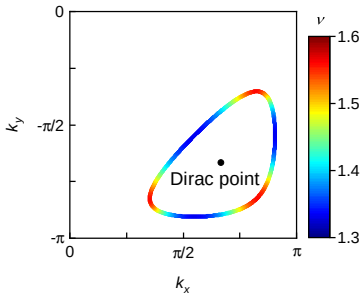

Supplementary Figure S2. The values of (k_x, k_y) from Eq. (S15) form a loop, with the color indicating the corresponding value of ν calculated from Eq. (S16). The black dot represents the Dirac point for a Hermitian Chern insulator with $\delta\nu = 0$.

Here, we have defined $C_{\mathrm{A,B}} = C_{\mathrm{g}} \pm \delta C$ and $\nu_{1,2} = \nu \pm \delta\nu$. To obtain the frequency band structure, we set the external currents to zero, leading to the equation

$$\mathbf{H}\begin{pmatrix} -i\omega\mathbf{V} \\ \mathbf{V} \end{pmatrix} = \omega \begin{pmatrix} -i\omega\mathbf{V} \\ \mathbf{V} \end{pmatrix}. \tag{S8}$$

In this context, the Hamiltonian is given by

$$\mathbf{H} = -i\begin{pmatrix} \mathbf{C}^{-1}\mathbf{\Sigma} & \mathbf{C}^{-1}\mathbf{L} \\ -\mathbf{1} & \mathbf{0} \end{pmatrix}. \tag{S9}$$

When $\delta\nu = 0$, we have $d_3 = -\omega\delta C + \frac{2\nu}{R}\left[\sin k_x - \sin k_y - \sin\left(k_x - k_y\right)\right]$. At the high-symmetry points $\mathbf{K} = \left(\frac{2}{3}\pi, -\frac{2}{3}\pi\right)$ and $\mathbf{K}' = \left(-\frac{2}{3}\pi, \frac{2}{3}\pi\right)$, we find that $d_1 = d_2 = 0$ and $d_3 = -\omega\delta C \pm 3\sqrt{3}\frac{\nu}{R}$. Thus, the phase transition boundaries are characterized by $\nu_{\pm} = \pm\frac{\omega\delta C R}{3\sqrt{3}}$. In the non-Hermitian case where $\delta\nu \neq 0$, a line gap occurs in the complex frequency plane, and the center of this line gap can be obtained by setting $d_0 = 0$. When $R_{\mathrm{g}} = \infty$, we have $f_0 = \frac{1}{2\pi\sqrt{L_{\mathrm{g}}(C_{\mathrm{g}}+3C)}}$. Since the phase diagram is symmetric with respect to $\nu = 0$, we only show the positive part with $\nu > 0$ in Fig. 2a.

Supplementary Note 2. Calculation of Chern numbers. In the regimes of trivial insulators and Chern insulators with line gaps in their band structures, Chern numbers are well defined. The non-Hermitian Chern number can be calculated as

$$C = \frac{1}{2\pi}\int_{\mathrm{BZ}} \mathbf{F}\left(\mathbf{k}\right)\cdot d^2\mathbf{k}, \tag{S10}$$

where $\mathbf{F}(\mathbf{k}) = \nabla \times \mathbf{A}(\mathbf{k})$ is the non-Hermitian Berry curvature, and $\mathbf{A}(\mathbf{k}) = -i\left\langle\psi^L\right|\partial_{\mathbf{k}}\left|\psi^R\right\rangle$ is the non-Hermitian Berry connection. Here, $\left\langle\psi^L\right|$ and $\left|\psi^R\right\rangle$ denote the left and right eigenvectors, respectively [2]. For simplicity, we

calculate the Chern numbers using the admittance band structure, yielding results consistent with those derived from the frequency band structure [1]. For the lower band, the left and right eigenvectors are given by

$$\left|\psi^R\right\rangle = \frac{1}{\sqrt{2d\left(d-d_3\right)}}\begin{pmatrix} d_3-d \\ d_1+id_2 \end{pmatrix}, \tag{S11}$$

$$\left\langle\psi^L\right| = \frac{1}{\sqrt{2d\left(d-d_3\right)}}\begin{pmatrix} d_3-d & d_1-id_2 \end{pmatrix}, \tag{S12}$$

where $d=\sqrt{d_1^2+d_2^2+d_3^2}$. The left and right eigenvectors satisfy the biorthogonal condition $\left\langle\psi^L\right|\left.\psi^R\right\rangle=1$. Using the above formulas and Eqs. (S5)-(S7), we find that Fig. 2b corresponds to the trivial insulator with $C=0$, while Fig. 2d corresponds to the nontrivial Chern insulator with $C=-1$.

Supplementary Note 3. Existence of exceptional points. Considering the general case where $\mathrm{Im}(d_3)\neq 0$, the existence of exceptional points requires that

$$d_1^2+d_2^2-\mathrm{Im}\left(d_3\right)^2=0, \tag{S13}$$

$$\mathrm{Re}\left(d_3\right)=0. \tag{S14}$$

This leads to the expressions

$$\delta\nu=\frac{\omega CR}{2}\frac{\sqrt{3+2\cos k_x+2\cos k_y+2\cos\left(k_x-k_y\right)}}{3-\cos k_x-\cos k_y-\cos\left(k_x-k_y\right)}, \tag{S15}$$

$$\nu=\frac{\omega\delta CR}{2\left[\sin k_x-\sin k_y-\sin\left(k_x-k_y\right)\right]}. \tag{S16}$$

Here, the parameter ω is defined as $\omega=\frac{1}{\sqrt{L_{\mathrm{g}}(C_{\mathrm{g}}+3C)}}$. The first condition always holds. Specifically, for a Hermitian Chern insulator with $\delta\nu=0$ and $\nu>0$, we find $(k_x,k_y)=\left(\frac{2}{3}\pi,-\frac{2}{3}\pi\right)$ and $\nu=\frac{\omega\delta CR}{3\sqrt{3}}$. For a non-Hermitian Chern insulator with $\delta\nu=0.5$, the values of (k_x,k_y) from the first condition form a loop, as illustrated in Fig. S2, where the color corresponds to the value of ν calculated from the second condition. In the state depicted in Fig. 2f with $\nu=1.5$, there are six exceptional points.

Supplementary Note 4. Circuit fabrication and measurement. All the circuit elements are delicately selected to achieve the $\pm1\%$ tolerance. In the NICs, we use the operational amplifier LM6171, and the values of the resistors are determined by $R_{\mathrm{b,A}}/R_{\mathrm{a,A}}=\frac{\nu-\delta\nu}{\nu+\delta\nu}$, $R_{\mathrm{c,A}}=\frac{R}{\nu+\delta\nu}$, $R_{\mathrm{b,B}}/R_{\mathrm{a,B}}=\frac{\nu+\delta\nu}{\nu-\delta\nu}$, and $R_{\mathrm{c,B}}=\frac{R}{\nu-\delta\nu}$. The resistors in the NICs are: (1) $R_{\mathrm{a,A}}=R_{\mathrm{b,A}}=1$ kΩ, $R_{\mathrm{c,A}}=680$ Ω, $R_{\mathrm{a,B}}=R_{\mathrm{b,B}}=1$ kΩ, and $R_{\mathrm{c,B}}=680$ Ω in Figs. 3a-b, Figs. 3e-f, Figs. 4a-b, and Figs. 4e-f; (2) $R_{\mathrm{a,A}}=1$ kΩ, $R_{\mathrm{b,A}}=872.7$ Ω, $R_{\mathrm{c,A}}=636.7$ Ω, $R_{\mathrm{a,B}}=872.7$ Ω, $R_{\mathrm{b,B}}=1$ kΩ, and $R_{\mathrm{c,B}}=729.6$ Ω in Figs. 3c-d and Figs. 3g-h; (3) $R_{\mathrm{a,A}}=1$ kΩ, $R_{\mathrm{b,A}}=355$ Ω, $R_{\mathrm{c,A}}=460.7$ Ω, $R_{\mathrm{a,B}}=355$ Ω, $R_{\mathrm{b,B}}=1$ kΩ, and $R_{\mathrm{c,B}}=1297.7$ Ω in Figs. 4c-d and Figs. 4g-h. High-Q inductors are used to reduce the parasitic loss.

The NICs are connected to a ±5 V DC power supply. A 4192A LF Impedance Analyzer, equipped with a splitter, is used to measure the voltage distributions across the circuit nodes. The output port of the impedance analyzer is connected to a 10 kΩ resistor, while the internal resistances of the channel ports are 1 MΩ. Under excitation, the eigenstates (both bulk and edge states) of the circuit lattice are activated. The coordinates for the excitation nodes at the left and right edges of the circuit lattice are $(0.5,3)$ and $(6,3)$, respectively. After probing the voltages at all nodes with a frequency step of 100 Hz, the complex voltages in real space are transformed into reciprocal space using a Fourier transform.

Supplementary Note 5. Robustness of non-Hermitian edge states. To investigate the robustness of the non-Hermitian edge states illustrated in Fig. 3, we first introduce circuit defects by grounding the nodes $(0.5,4)$, $(1,4)$, $(0.5,5)$, and $(1,5)$, which correspond to the left edge of the circuit lattice. As shown in Fig. S3a, the voltage spectra for the non-Hermitian Chern insulator phases with and without defects reveal that the amplifying edge state residing at the left edge is robust. Similarly, we create circuit defects by grounding the nodes $(5.5,2)$, $(6,2)$, $(5.5,1)$, and $(6,1)$, which correspond to the right edge of the circuit lattice. From Fig. S3b, we observe that the dissipative edge state residing at the right edge is also robust.

Fig. S4 illustrates the robustness of the non-Hermitian edge states presented in Fig. 4. Despite an increase in the strength of non-Hermicity, both the amplifying and dissipative edge states remain robust.

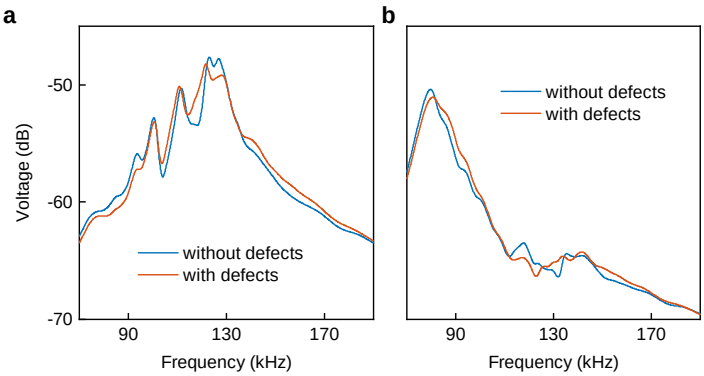

Supplementary Figure S3. Robustness of the (**a**) amplifying and (**b**) dissipative edge states shown in Fig. 3. The voltage spectra for the Chern insulator phase without defects are included for comparison.

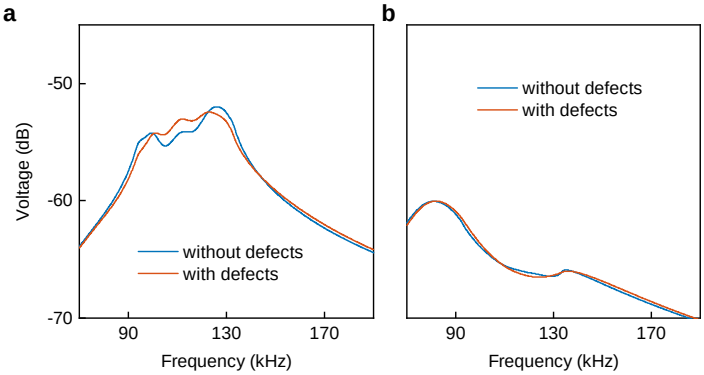

Supplementary Figure S4. Robustness of the (**a**) amplifying and (**b**) dissipative edge states depicted in Fig. 4.

* Corresponding author: rujiangli@xidian.edu.cn
† Corresponding author: coldfire2000@mail.xjtu.edu.cn

[1] Hofmann, T., Helbig, T., Lee, C. H., Greiter, M. & Thomale, R. Chiral Voltage Propagation and Calibration in a Topolectrical Chern Circuit. Phys. Rev. Lett. 122, 247702 (2019).
[2] Ezawa, M. Electric circuits for non-Hermitian Chern insulators. Phys. Rev. B 100, 081401 (2019).